nature communications

Article

https://doi.org/10.1038/s41467-025-59878-w

Dynamic single-cell metabolomics reveals cell-cell interaction between tumor cells and macrophages

Received: 5 September 2024

Accepted: 8 May 2025

Published online: 16 May 2025

Check for updates

Yi Zhang, Mingying Shi, Mingxuan Li, Shaojie Qin, Daiyu Miao & Yu Bai

Single-cell metabolomics reveals cell heterogeneity and elucidates intracellular molecular mechanisms. However, general concentration measurement of metabolites can only provide a static delineation of metabolomics, lacking the metabolic activity information of biological pathways. Herein, we develop a universal system for dynamic metabolomics by stable isotope tracing at the single-cell level. This system comprises a high-throughput single-cell data acquisition platform and an untargeted isotope tracing data processing platform, providing an integrated workflow for dynamic metabolomics of single cells. This system enables the global activity profiling and flow analysis of interlaced metabolic networks at the single-cell level and reveals heterogeneous metabolic activities among single cells. The significance of activity profiling is underscored by a 2-deoxyglucose inhibition model, demonstrating delicate metabolic alteration within single cells which cannot reflected by concentration analysis. Significantly, the system combined with a neural network model enables the metabolomic profiling of direct co-cultured tumor cells and macrophages. This reveals intricate cell-cell interaction mechanisms within the tumor microenvironment and firstly identifies versatile polarization subtypes of tumor-associated macrophages based on their metabolic signatures, which is in line with the renewed diversity atlas of macrophages from single-cell RNA-sequencing. The developed system facilitates a comprehensive understanding single-cell metabolomics from both static and dynamic perspectives.

Metabolomic analysis uncovers the chemical phenotype of human subjects, and metabolic dysregulation often causes cellular malfunctions and plays a pivotal role in the pathogenesis and progression of diseases[1,2]. Measurement of concentrations of metabolites, however, can only provide a "snapshot" of metabolic status, which represents the converged results of multiple metabolic reactions, including the production and consumption with various flow orientations[3,4]. It indicates that high metabolite's concentrations not usually represent for high reaction flux, since the accumulation of metabolites may attribute to the decreased consumption[5]. Hence, the analysis of metabolic activity is of greater significance than metabolic concentration information in enabling us to ascertain the dynamics of metabolic pathways and delineate the interconnected metabolic network, such as various nutrient origins. Stable isotope tracing metabolomics is an attractive tool for determining metabolic activity[3,6], during which cells or organisms are administered with stable isotope tracers such as [U-^{13}C]-glucose and their transformation into labeled metabolites through the metabolic network is subsequently tracked[7,8]. Thus, the activity of metabolites and pathways can be unraveled through the labeling form and labeling extent (LE), which represents the enrichment of all labeling forms of the metabolite (see "Method"). Targeted isotope tracing metabolomics enables the observation of specific

Beijing National Laboratory for Molecular Sciences, Key Laboratory of Bioorganic Chemistry and Molecular Engineering of Ministry of Education, College of Chemistry and Molecular Engineering, Peking University, Beijing, China. e-mail: yu.bai@pku.edu.cn

pathway activities to reveal underlying biological mechanisms[8–10]. However, this approach is constrained by a limited number of labeled metabolites and lacks comprehensive analysis of global homeostasis. In recent years, untargeted isotope tracing metabolomic methodologies have also emerged to facilitate comprehensive delineation of metabolic activities across the entire system and provide opportunities for the discovery of novel pathways[11–13]. Nevertheless, the intricate isotope-labeled data pose significant challenges for data processing and interpretation, necessitating the utilization of sophisticated algorithms and models.

Compared with general metabolomics, single-cell metabolomics reveals the widely existed cell heterogeneity under typical physiological status[14–16] as well as various cell subtypes across the organs or tumors. In complex microenvironments, cell metabolism is influenced by neighboring cells through cell-cell communication, which relies on the secretion of soluble molecules[17], extracellular vesicles[18], or the formation of tumor microtubes[19]. Conventional population analysis of co-cultured cells typically depends on indirect co-cultured systems separated by a membrane[20], while direct co-cultured methods require inevitable labeling to isolate cells for subsequent analysis, such as Fluorescence-activated Cell Sorting (FACS), which might induce impact on the cellular metabolomics[21,22]. Single-cell metabolomics can exactly solve these problems by enabling direct co-culture of different cell types to more accurately mimic physiological conditions, and allowing for the direct analysis of single cells without any labeling for in vitro cell-cell interaction studies. Efforts have been made towards single-cell-based in situ studies of cell-cell communication[23,24], with ongoing work focused on developing label-free and high-throughput single-cell metabolomics analysis methods for this purpose. Recently, there is an emergence of isotope tracing analysis on tissues using mass spectrometry imaging (MSI) at near single-cell resolution[25–28]. It reveals the spatial organization of metabolic activity, underscoring the significance of analyzing metabolic activity at the single-cell level. However, a limited number of identified metabolites resulting from matrix effect, delocalization of metabolites, and challenges in single-cell segmentation from pixels causes difficulties for single-cell heterogeneous analysis. Especially, it is not suitable for conducting analysis of live single-cells, those are crucial for evaluating the metabolic activity. Online single-cell metabolomic sampling such as organic mass cytometry[29,30] and CyESI[31] are recently developed technologies for single-cell metabolomic analysis with minimal sample pretreatment and high single-cell throughput, unveiling precisely cell typing and metabolomic changes at different biological conditions[32–35]. Importantly, this approach enables the direct detection of hundreds of metabolites from single cells at physiological condition[36], circumventing matrix deposition and complex single-cell segmentation in MSI. Therefore, organic mass cytometry serves as a potential tool for single-cell metabolic activity analysis, which has not been previously explored. Besides the methodologies for single-cell isotope tracing analysis, the data processing method also remains challenging. The peaks extraction methods using one cell marker in existing organic mass cytometry analysis may cause false-positive identification and biased peak quantification of metabolites. Meanwhile, there is an urgent need to develop a compatible untargeted isotope tracing analysis platform for single-cell data.

In this study, we develop a universal dynamic single-cell metabolomic analysis system by integrating a single-cell metabolomic analysis platform and untargeted stable isotope tracing analysis, enabling dynamic metabolomics of single cells in a high-throughput and label-free way (Fig. 1). Organic mass cytometry is utilized for single-cell data acquisition due to its high single-cell throughput. Then, the data processing workflow for untargeted single-cell metabolomics and targeted extraction of isotopically labeled metabolites is constructed. A delicate data processing by a homemade Python program is developed for rational single-cell data extraction and automated quantification of LE and labeling patterns of all labeled metabolites in single cells. Subsequently, system-wide metabolic activity analysis is achieved by the model cell line MDA-MB-231 with 40 labeled metabolites. Different metabolic activities are determined, and interconnected pathways with various cycles and flow orientations are observed at the single-cell level. Heterogeneous metabolic activities within single MDA-MB-231 cells were also demonstrated using this method. We further discover the activity alteration of glycolysis as well as other pathways across different 2-deoxyglucose (2-DG) induced conditions, which indicates more precisely cell typing with metabolic activity information of single cells. Importantly, the developed system is utilized for the study of cell-cell interaction of directly co-cultured tumor cells and macrophages with the aid of a machine learning model for online cell type identification, revealing significant metabolic alteration of these two cell types in both concentration and activity. The versatile subtyping of tumor-associated macrophages (TAM) reveals cell heterogeneity featured with differential metabolic alterations in the tumor microenvironment (TME). In summary, our dynamic single-cell metabolomics system enables determination of metabolic activities and delineation of crosslinked metabolic networks, thus provides deeper single-cell metabolomic analysis which holds great potential for further exploration in cell heterogeneity and cell-cell communication.

Results

Construction of dynamic single-cell metabolomics system

In order to achieve the high-throughput dynamic metabolomic analysis of single cells, a single-cell metabolomics platform was constructed through combining the idea of organic mass cytometry with isotope tracing. In this work, a high-throughput organic mass cytometry device was constructed through coupling CyESI-MS to Dean flow-based single-cell dispersion[37] (Supplementary Fig. 1a, b). The chromatography of single cell pulse was demonstrated in Supplementary Fig. 1c, and fine subtyping of 3 cell lines including MCF10A, MCF-7 and MDA-MB-231 were demonstrated to verify its capability for discrimination between normal epithelial cells and cancer cells, as well as subtyping of different breast cancer cells (Supplementary Fig. 1d). Internal standard (IS) of 2-Chloro-L-phenylalanin was added to the sheath liquid during data acquisition, and high stability of the device was validated from the low relative standard deviation (RSD) of IS intensity (7.8%), while high RSD was observed in the relative intensity of endogenous metabolites in single cells (Supplementary Fig. 2a), confirming the cell heterogenous detected by the device. Robustness of the device was also confirmed by 3 replicate acquisitions (Supplementary Fig. 2b). Stable isotope tracing was introduced to this platform to achieve a high-throughput dynamic metabolomic data acquisition. Subsequently, in order to achieve a global dynamic profiling of single cells, the single-cell compatible analysis workflow of isotope tracing analysis was generated according to recently developed MetTracer technology, which was built for global isotope tracing of bulk system[38] (Fig. 2a). Firstly, both labeled and unlabeled samples were analyzed by organic mass cytometry. Untargeted metabolomics were conducted for unlabeled single cells, wherein metabolite annotation was achieved through matching the accurate mass with the standards in Human Metabolome Database (HMDB) as well as the local database constructed from LC-MS/MS from population cells and online single-cell MS/MS analysis[36] (see “Methods”, Supplementary Fig. 3 and Supplementary Data 1). Subsequently, the corresponding isotopologue peaks library of the annotated metabolites was constructed. Meanwhile, all of the detected peaks in labeled samples were screened for single-cell characteristic pulse peaks (see “Methods”), leading to the determination of characteristic peaks of single cells. Then, the targeted extraction of potential isotopologue peaks from the characteristic peaks in labeled single cells was performed, and the specific labeled isotopologue peaks and corresponding labeled

https://doi.org/10.1038/s41467-025-59878-w

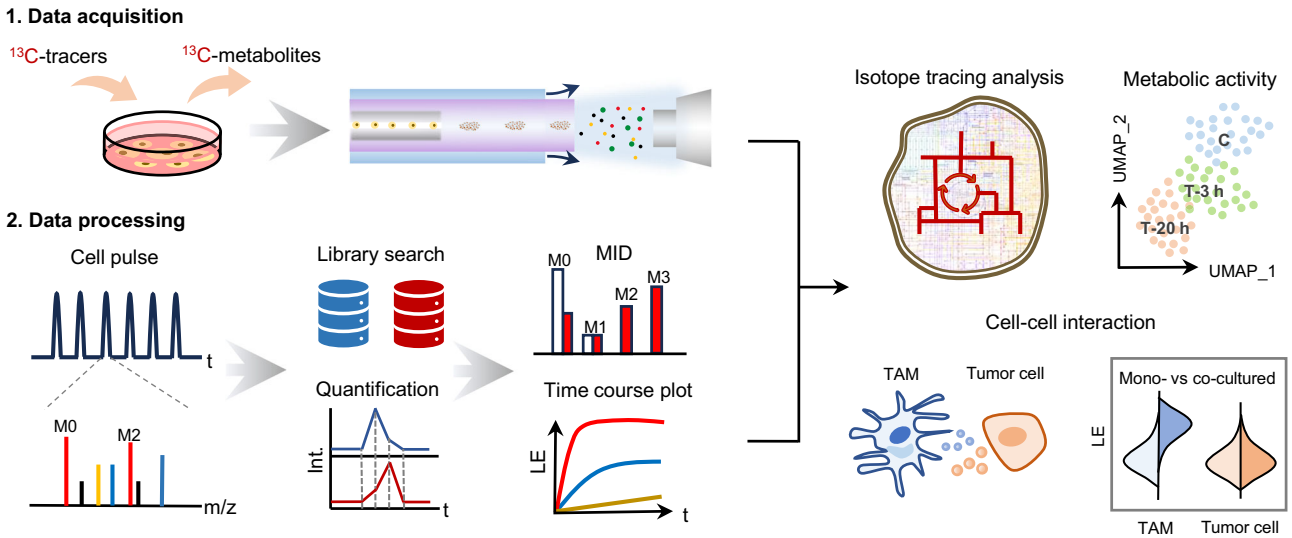

Fig. 1 | Schematic workflow of the dynamic single-cell metabolomics system. Cells were labeled with isotope tracers and analyzed using the high-throughput data acquisition platform. Subsequently, the single-cell essential metabolic data processing and isotope tracing analysis were performed by a Python-based data processing platform. This system enables profiling of metabolic activity and flow analysis of interlaced metabolic networks at the single-cell level, which was further applied in the study of cell-cell interaction.

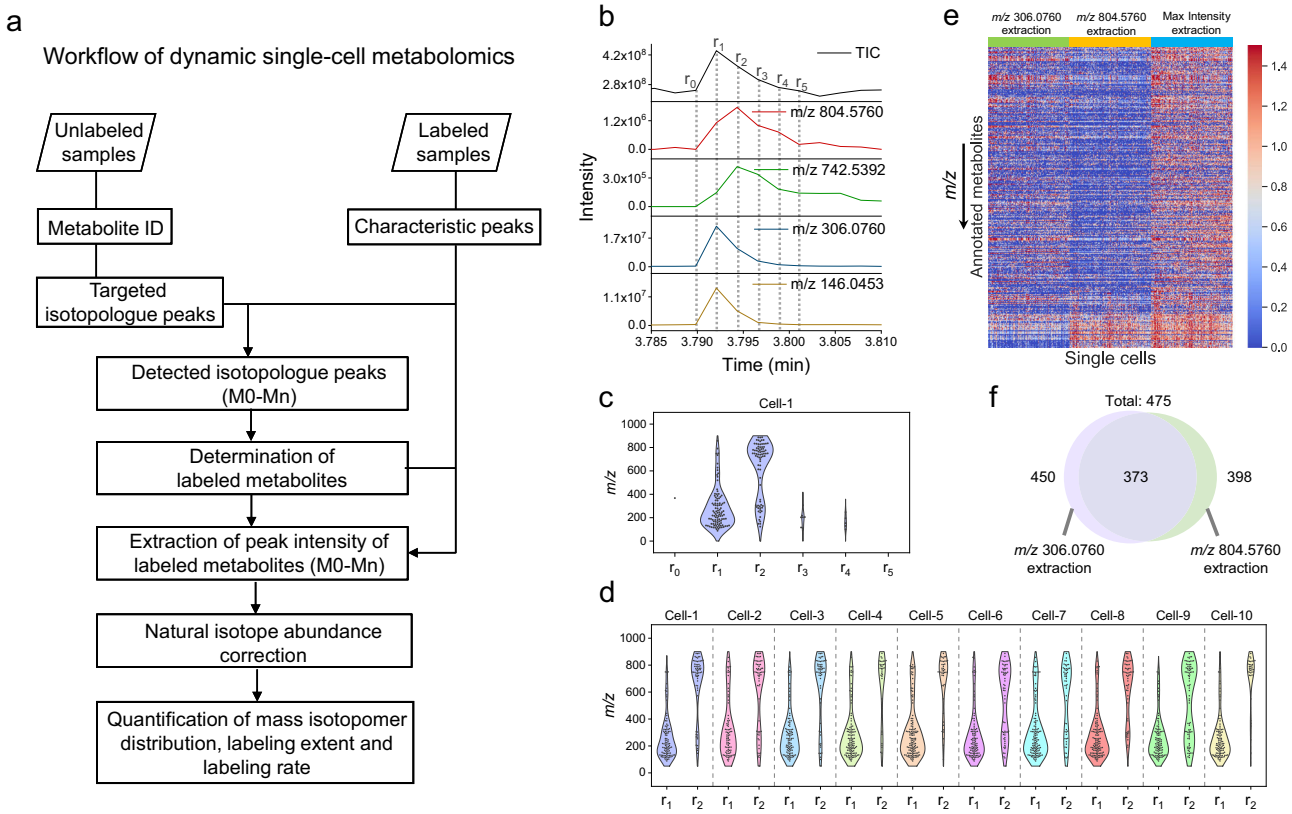

Fig. 2 | Dynamic single-cell metabolomics data processing platform. a Data processing workflow of untargeted dynamic single-cell metabolomic analysis. **b** Total ion chromatography (TIC) and extract ion chromatography (EIC) of cell markers in one cell pulse. **c** The RT distribution of maximum intensity of metabolites during one cell pulse (r_0-r_5). **d** The r_1/r_2 distribution of maximum intensity of metabolites with different *m/z* values in 10 single cells. **e** The heatmap of metabolites' relative intensities extracted by a specific cell marker or the maximum intensity. The data was normalized by the mean values of each *m/z*. **f** The Venn plot of annotated metabolites extracted by two cell markers, respectively. The analyzed cell line is MDA-MB-231. Cell number = 188. Source data are provided as a Source Data file.

metabolites can be determined. Then, all labeled isotopologue peaks' intensities were extracted and correction for natural isotope abundance. Finally, the LE of M0-Mn of metabolites in each single cells were calculated, with the output of statistical analysis figures, including mass isotopomer distribution (MID), time-course fitting curve of averaged LE, and distribution of heterogeneous LE of single cells. The entire data processing pipeline was executed using a homemade Python program, offering an efficient and streamlined workflow for essential single-cell data processing and isotope tracing analysis.

Specifically, the essential single-cell data processing before isotope tracing analysis includes single-cell pulse peak selection, characteristic peak determination, metabolite annotation, and peak intensity extraction. It can be observed that a single cell pulse includes 3-6 mass spectra indicated by TIC variation and EIC of cell markers under our data acquisition conditions (Fig. 2b). The retention time (RT) of maximum intensity of glutathione (*m/z* 306.0760) was marked as r_1 for one cell pulse, and the RTs of the adjacent 6 spectra within this cell pulse were respectively annotated as r_0 - r_5, as presented in Fig. 2b. The difference of spectrum numbers between cells may attribute to various cell volume, and the difference between metabolites may result from different intracellular concentration and extraction efficiency of metabolites by the sheath liquid. In a subset of cells (about 2/3), the peak intensity of various metabolites reached their maximum at different time points during the cell pulse, which may attribute to microelectrophoresis separation (at the timescale of millisecond)[39,40] following the metabolites extraction from the single cell during the contact with methanol (~ 0.86 s[31]) at the spray tip (Fig. 2b). We investigated the RT of maximum intensity for cell characteristic peaks in 10 cell pulses and observed that the majority of these peaks reach their maximum intensity at two adjacent spectra (time interval of 135 ms) within the cell pulse, specifically r_1 and r_2 (Fig. 2c, d). Furthermore, it can be observed that peaks within the *m/z* range of 80-500 tend to exhibit maximum intensity earlier at r_1, while those within the *m/z* range of 500–1000 preferentially display maximum intensity later at r_2 (Fig. 2d). These findings are consistent with the electromigration rates of molecules with different sizes. We draw the heatmap of single-cell metabolites' intensities extracted by *m/z* 306.0760 (glutathione), *m/z* 804.5760 (PS (37:0)) and maximum intensity in each cell pulse respectively, and significantly different metabolic profiling was observed (Fig. 2e). Therefore, the maximum intensity of each detected peak in each cell pulses was extracted separately to avoid the biased quantification based solely on one cell marker. Actually, more metabolites can be determined through two cell markers with different molecular weights than using only one (Fig. 2f). In addition, the signal-to-blank ratio (SBR) of each detected peak was calculated through the maximum intensity within the cell pulse divided by the adjacent background intensity, and only *m/z* peaks with SBR > 3 and occurrence frequency > 20% of all cells were kept as characteristic peaks of cells and used for further processing (see "Methods"). In conclusion, an isotope tracing-based organic mass cytometry platform was constructed for the acquisition of single-cell dynamic metabolomic data, and a streamlined data processing platform was developed for the processing of essential single-cell data and untargeted isotope tracing analysis.

Global metabolic activity profiling at the single-cell level

As a proof-of-concept, we demonstrated the global single-cell metabolic activity profiling using above developed system on the MDA-MB-231 cell line (Fig. 3a). The cells were cultured in medium with dialysis fetal bovine serum (dFBS), and labeled by [U-^{13}C]-glucose or [U-^{13}C]-glutamine separately for 5 min to 3 h labeling time after optimization. Cells were then collected and dispersed by trypsin, and prepared for organic mass cytometry analysis. A comparison between trypsinization and scraping for cell harvest was carried out for bulk cells, and the results indicated that there was no significant difference in the determination of metabolic activity for 98% of the metabolites between them (Supplementary Fig. 4). 32 and 23 of labeled metabolites were determined through the isotope tracer of glucose and glutamine, respectively, result in a total of 40 metabolites labeled within 3 h (Fig. 3b and Supplementary Data 2). The KEGG enrichment analysis indicated that some pathways were prone to be labeled and detected by our method (Fig. 3c), such as alanine, aspartate, and glutamate metabolism, arginine biosynthesis, TCA cycle, purine metabolism, ascorbate and aldarate metabolism, etc. These labeled metabolites demonstrated different LE and labeling rates, which indicated different metabolic activities. Although we can't monitor the LE changes in one individual cell because of the "destructive detection" of mass cytometry, we can acquire the averaged LE in hundreds of single cells at each time point as displayed in Fig. 3d. The averaged isotope tracing results of single cells were compared to LC-MS analysis of population cells, and averaged LE and MID of represent metabolites were demonstrated in Supplementary Fig. 5, indicating the basic consistency between averaged single-cell results and population cells. Further, the labeled metabolites were hierarchically clustered into 3 clusters under glucose or glutamine labeling conditions (Fig. 3d), and diverse time-course patterns of these clusters were obtained (Fig. 3e, f). Metabolites in cluster 1 reached isotopic steady state within 3 h labeling, with the highest labeling rate. While, metabolites in clusters 2 and 3 could not reach isotopic steady state in 3 h with step down labeling rates. Nonlinear fittings of each metabolite were conducted, and the calculated labeling rates (k, see "Methods") of metabolites in 3 clusters (Fig. 3g, h) were in consistent with the time-course patterns. The performance of the above two isotope tracers were demonstrated separately, and KEGG annotations of notable labeled pathways in each cluster were displayed (Fig. 3i, j). For instance, the galactose metabolism and sphingolipid metabolism showed high labeling rates by glucose labeling, meanwhile, the glutamine labeling showed high labeling rates in alanine, aspartate and glutamate metabolism and histidine metabolism. In summary, we demonstrated the isotope tracing and metabolic kinetic analysis using our method, and a global delineation of metabolic activity can be drawn by the wide-coverage labeling and untargeted isotope tracing analysis at the single-cell level.

Apart from average analysis, the cellular heterogeneity of metabolic activity was also demonstrated using our method. We collected single-cell isotope tracing data labeling by [U-^{13}C]-glucose, with a total of approximately 5000 single cells from 6 labeling time points. Uniform Manifold Approximation and Projection (UMAP) analysis based on the LE features of all single cells was conducted, and subclusters of single cells emerged (Fig. 4a). Density Based Spatial Clustering of Applications with Noise (DBSCAN) was performed on the total cells, resulting in 6 clusters, namely A, B, C, D, E, and F (Fig. 4b). The LE of labeled metabolites in clusters A–F was analyzed (Supplementary Fig. 6), and an increase in LE from A to F in each labeled metabolite was observed, indicating an evolution along clusters A–F as the labeling time progresses (Fig. 4b). The distribution of single cells from each time-course group is displayed in Fig. 4c. It can be noted that the cluster population varies at different time points, and there were more than one subcluster of A–F in many time-course groups, including 5 min, 10 min, 30 min, 1 h and 3 h. These results reveal the heterogeneous metabolic activities and the non-synchronous of single cells over labeling time, which cannot be captured in bulk analysis.

Interconnection and flow analysis of metabolic pathways at the single-cell level

Metabolic pathways form a complex, interconnected network within cells, and a single metabolite can be influenced by multiple pathways. Isotope labeling-based dynamic single-cell metabolomics not only offers insights into metabolic activity but also reveals diverse pathways in which a metabolite participates. Here, various pathways and their interconnections can be observed through the labeling patterns of

https://doi.org/10.1038/s41467-025-59878-w

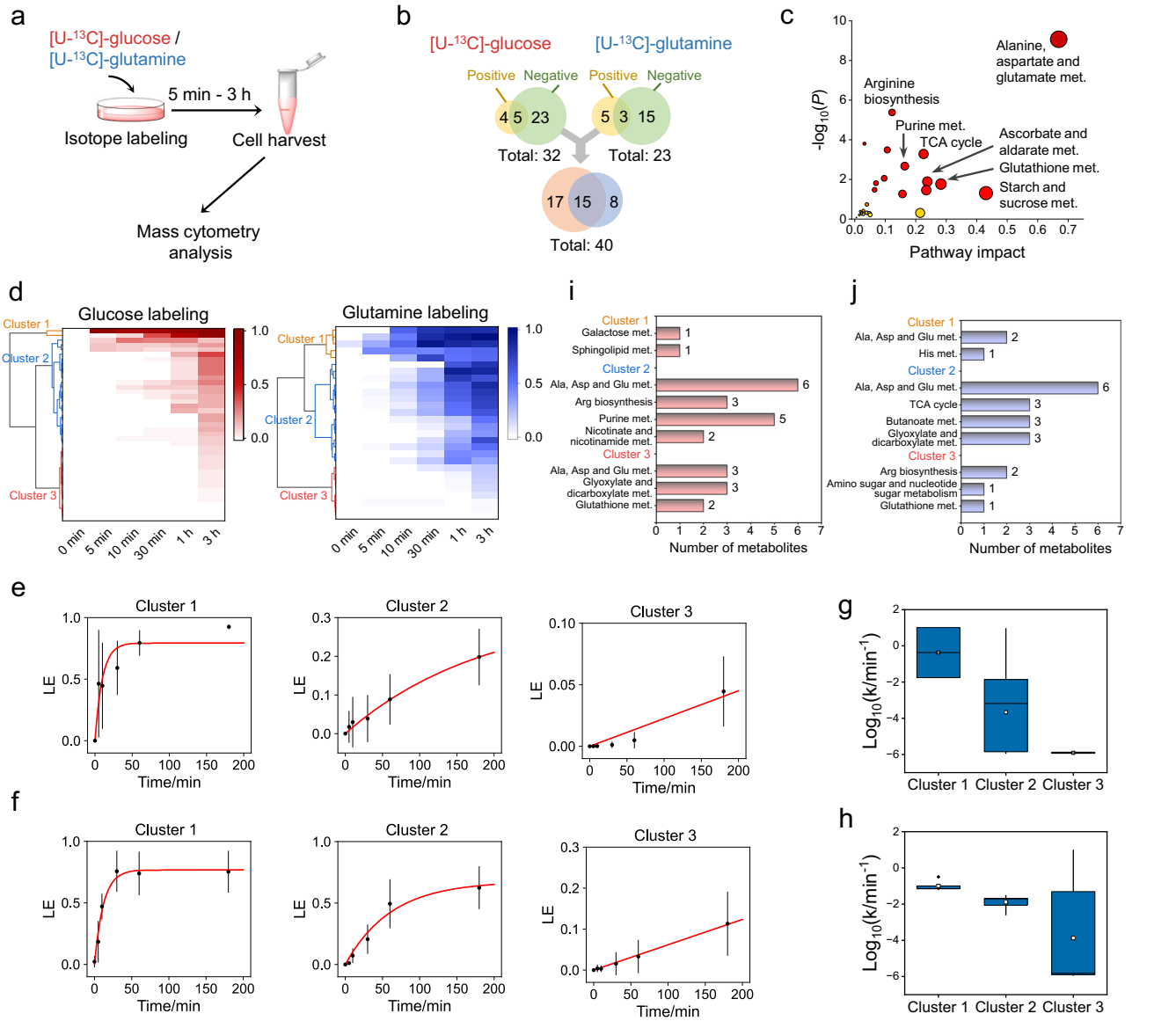

Fig. 3 | Global single-cell metabolic activity profiling. a Schematic illustration of isotope labeling of cells and mass cytometry analysis. **b** The Venn plot of labeled metabolites detected under the negative and positive modes labeled by [U-^{13}C]-glucose and [U-^{13}C]-glutamine separately. **c** The KEGG enrichment analysis of labeled metabolites. **d** Hierarchical-clustering analysis of metabolites' averaged LE at different time point. **e**, **f** The time-course plot of metabolites' LE in 3 clusters labeled by the tracer (**e**) [U-^{13}C]-glucose and (**f**) [U-^{13}C]-glutamine. Data are presented as mean values (black dots) +/− SD. The red line is the exponential fitting line. **g**, **h** The box plot of logarithmic transformed labeling rates of each metabolite in 3 clusters labeled by (**g**) [U-^{13}C]-glucose and (**h**) [U-^{13}C]-glutamine. The centerlines of the boxplots indicate the median values, the lower and upper lines in boxplots correspond to 0.25 and 0.75 quartiles, and the whiskers indicate the largest and lowest points inside the range defined by 0.25 and 0.75 quartile plus 1.5 times the interquartile range (IQR). The white point represents mean values. **i**, **j** The KEGG annotation of metabolites in 3 clusters labeled by (**i**) [U-^{13}C]-glucose and (**j**) [U-^{13}C]-glutamine. Cell number = 100 for each group. Source data are provided as a Source Data file.

metabolites. Cancer cells consume glucose at a surprisingly high rate compared to normal cells by aerobic glycolysis to meet the bioenergetics and biosynthesis needs for proliferation, a phenomenon termed "the Warburg effect"[41,42]. The glycolysis provides cells with intermediates for many biosynthetic pathways, thus the production rate of the associated metabolites indicated the glycolysis reaction rate to some extent. The time-course labeling of UDP-glucose/UDP-galactose was observed at the single-cell level using [U-^{13}C]-glucose as a tracer (Supplementary Fig. 7a and Supplementary Fig. 8a). The LE of M6 indicated the hexose of UDP-glucose was rapidly labeled (within 5 min) via the glucose-1P intermediate from the glycolysis pathway (Fig. 5a), while the M5-labeled ribose was generated later through the pentose phosphate pathway and pyrimidine metabolism, such as uridine (Supplementary Fig. 8b). Therefore, the M11 isotopelogue of UDP-glucose emerged after 1-hour labeling, with a significant decrease in LE of M6 after 3-hour labeling (Fig. 5b). In addition, the labeling pattern of UDP-GlcNAc indicated the interconnection of various pathways resulting in versatile labeled forms (Supplementary Fig. 8c, d). Pyruvate (M3) was produced following the uptake of [U-^{13}C]-glucose via the glycolysis pathway, and its involvement in the TCA cycle was observed (Supplementary Fig. 7b)[43]. Various labeled isotopologues were detected for metabolites participating in the TCA cycle, such as citrate, succinate, and malate (Fig. 5c and Supplementary Fig. 8e). The M2 isotopologues detected in succinate and malate indicated their involvement in the first TCA cycle from pyruvate through acetyl-CoA. Subsequently, M3 isotopologues were produced and detected in

https://doi.org/10.1038/s41467-025-59878-w

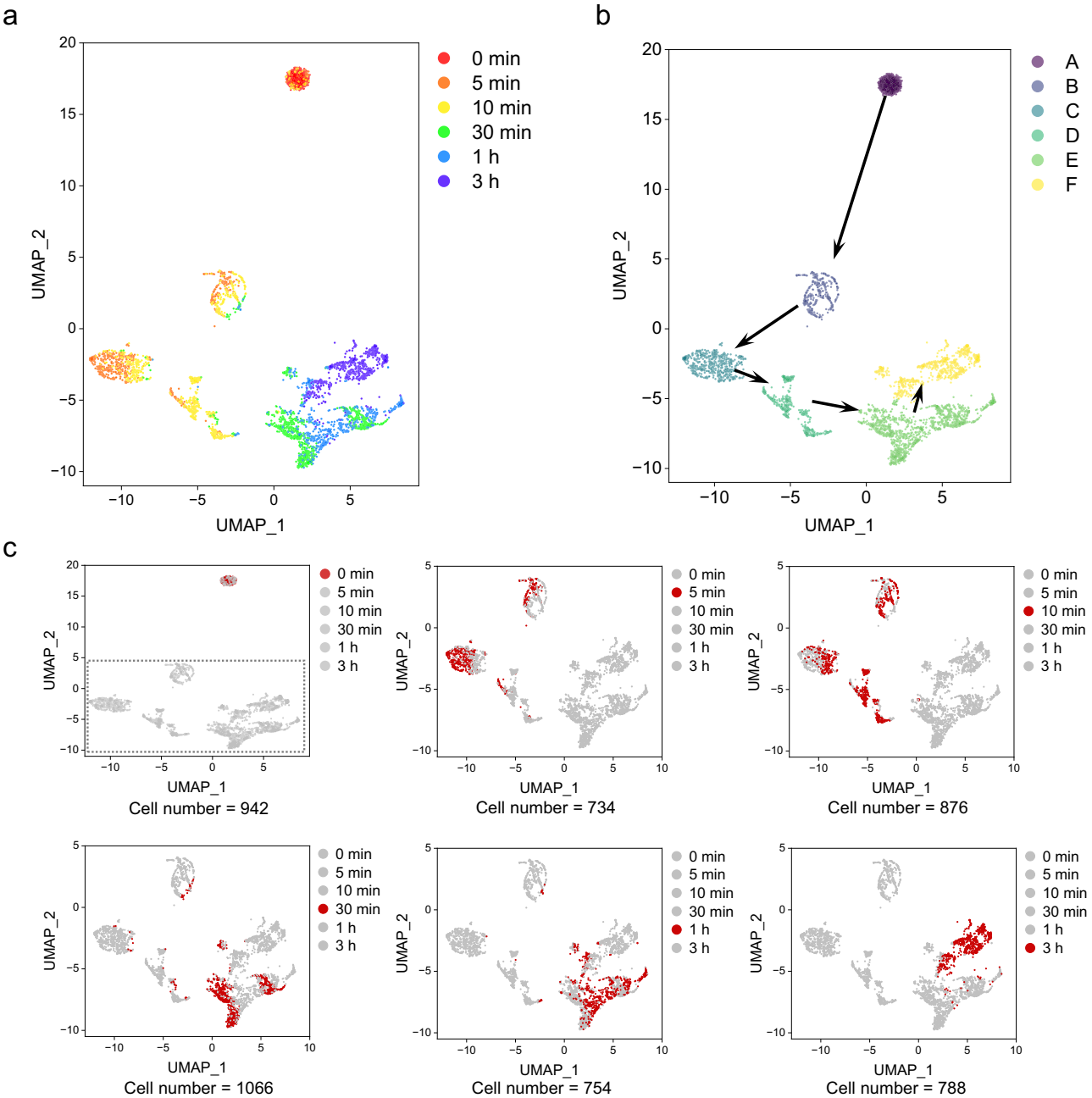

Fig. 4 | Cell heterogeneity of metabolic activity in single MDA-MB-231 cells. **a** UMAP analysis of single cells according to the LE of labeled metabolites after different labeling times by [U-^{13}C]-glucose. Z-score normalization. Total cell number = 5160. **b** DBSC cluster of total cells in (**a**) resulting in 6 subclusters, namely A–F. eps = 1, min_samples = 100. **c** Distribution of single cells in A–F subclusters from 6 groups of labeling time. The cell number of each group was annotated below each figure. The dotted box in the subfigure of the 0 min group was magnified in the other subfigures. Source data are provided as a Source Data file.

succinate and malate during the second TCA cycle. Apart from the second TCA cycle, M3 malate can be produced via pyruvate anaplerosis catalyzed by pyruvate carboxylate (PC) from pyruvate (Supplementary Fig. 7b), and the comparison between LE of M3 malate and M3 succinate indicated the pyruvate anaplerosis contribution to the TCA cycle[44] (Supplementary Fig. 9). The third TCA cycle resulted in the emergence of M4 isotopologues which were detected in succinate. Furthermore, metabolites associated with the TCA cycle such as aspartate and glutamate exhibited similar labeling patterns corresponding to different cycles within the TCA pathway (Fig. 5d). In addition, the platform enabled correlation matrix analysis of labeling patterns in single cells, and it was conducted for 3-hour labeling samples (Fig. 5e). The correlation matrix analysis revealed in-depth pathway correlations in single cells (Fig. 5f), including a positive correlation between M11 labeled UDP-glucose and ribose in the pyrimidine pathway, a positive correlation between M6 labeled UDP-glucose and other pyrimidine nucleotide sugars (UDP-GlcNAc, UDP-D-Glucuronate), and a positive correlation among various isotopologues of UDP-GlcNAc. The correlation matrix also revealed the significant positive correlation among the TCA-related metabolites as well as between different TCA cycles (Fig. 5f and Supplementary Fig. 10).

Additional isotope tracers were utilized to observe biological reversible or multiplex pathways at the single-cell level. It has been reported that lactate can be utilized by lung cancer cells via gluconeogenesis as an alternative energy source to adapt to glucose depletion[45]. Therefore, [U-^{13}C]-glucose and [U-^{13}C]-lactate were

https://doi.org/10.1038/s41467-025-59878-w

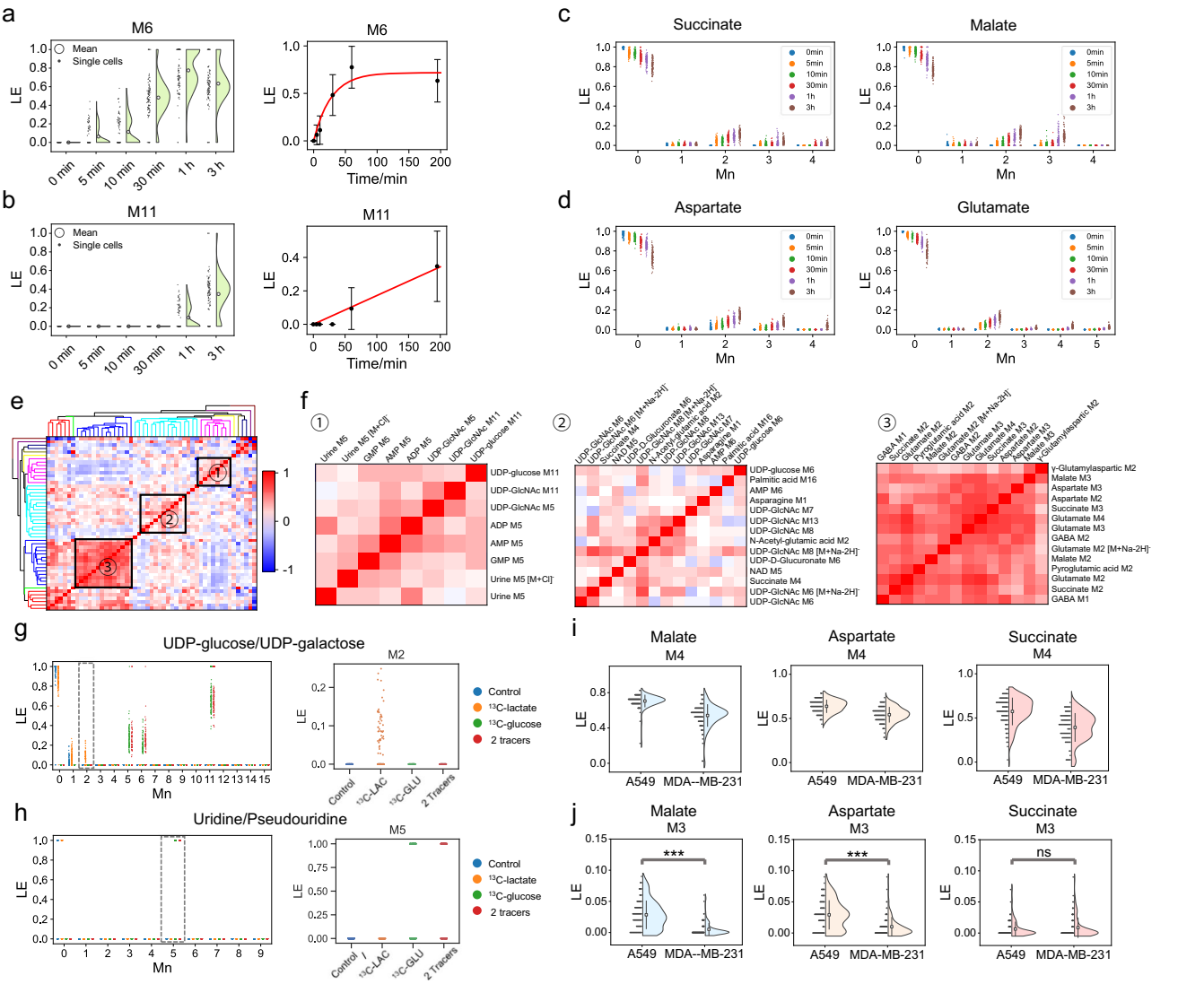

Fig. 5 | Metabolic flow and interconnection via versatile labeling tracers at the single-cell level. a, **b** The time-course labeling patterns of (**a**) M6 and (**b**) M11 labeled UDP-glucose/UDP-galactose. The left panels are the violin plots of single cells. Right panels are presented as averaged LE (black dots) +/- SD, and the red line represents the exponential fitting line. Cell number = 100 for each group. **c**, **d** The time-course labeling patterns of (**c**) TCA intermediates and (**d**) associated metabolites. Cell number = 100 for each group. **e** The correlation matrix of LE after 3 h labeling. The Pearson correlation coefficient was calculated with the exclusion of all single cells containing zero values. **f** Enlarged figures of the correlation matrix corresponding to **e**. Cell number = 268. **g**, **h** The labeling patterns of (**g**) UDP-glucose/UDP-galactose and (**h**) uridine/pseudouridine after 12 h labeling. The right panel is the enlarged view of a specific labeled form in the left panel. The blue, orange, green, and red dots present samples of unlabeled, [U-^{13}C]-lactate labeling, [U-^{13}C]-glucose labeling, and co-labeling of the above 2 tracers, respectively. Cell number = 200 for each group. **i**, **j** The LE of (**i**) M4 and (**j**) M3 labeled metabolites after 3 h labeling by [U-^{13}C]-glutamine in A549 and MDA-MB-231 cell lines. Data are presented as mean values +/− SD, and black dots represent single cells. A two-sided Wilcoxon rank-sum test was performed to assess significance, and $P = 1.61 \times 10^{-15}$, 6.44×10^{-9}, 9.269×10^{-1} for M3 malate, M3 aspartate, and M3 succinate, respectively. ***$P < 0.001$; ns non-significant. Cell number = 100 for each group. Source data are provided as a Source Data file.

selected as tracers to track the glycolysis and gluconeogenesis pathways, and UDP-glucose/UDP-galactose was chosen as the readout of upper pathways[25] (Supplementary Fig. 7c). M6 and M11 labeled UDP-glucose were generated upon the entry of [U-^{13}C]-glucose into glycolysis, while the utilization of [U-^{13}C]-lactate as a tracer would result in a mixed isotope distribution pattern of downstream metabolites due to the labeled carbon loss through the TCA cycle[46], and M2 labeled UDP-glucose was observed when using [U-^{13}C]-lactate as the only tracer, probably attributing to the detection limit in single cells (Fig. 5g). Furthermore, absence of labeled uridine by [U-^{13}C]-lactate indicated that M2 labeled UDP-glucose originated from hexose labeling via gluconeogenesis (Fig. 5h). However, simultaneous labeling with [U-^{13}C]-glucose and [U-^{13}C]-lactate did not yield detection of the M2 isotopologue, which can be attributed to a faster labeling rate via glycolysis masking the labeling for fewer carbon atoms in hexose. When utilizing [U-^{13}C]-glutamine as the isotope tracer, α-ketoglutarate derived from glutamine can not only undergo oxidation in the TCA cycle through glutaminolysis, but also be transformed into citrate via the reductive glutamine metabolism particularly under hypoxic conditions (Supplementary Fig. 7d)[47,48]. The M4 labeled TCA intermediates, including malate, aspartate, and succinate, were produced through the TCA cycle and emerged as the predominant labeling form under normal culture conditions, with a higher labeling rate in A549 cell compared to MDA-MB-231 cell (Fig. 5i). The M3 isotopologues of these metabolites can be attribute to the reductive glutamine metabolism, with significantly higher LE of M3 labeled malate and aspartate in A549 cells compared to MDA-MB-231, indicating a higher reductive activity in A549 (Fig. 5j). Conversely, non-significant difference in LE of

M3 labeled succinates between the two cell lines can be attribute to a relatively low proportion of succinates origin from the reductive metabolism in A549, which consistent with earlier study results with population cells[47]. However, further verification using more specific isotope tracers tracking the reductive metabolism is necessary to avoid potential interference from impurities in [U-^{13}C]-glutamine and different TCA cycles leading to the emergence of M3 isomers at the single-cell level.

2-DG induced metabolic perturbations in single MDA-MB-231 cells

2-DG is a synthetic analog of glucose, in which the 2-hydroxyl group is replaced by hydrogen. It functions as a chemotherapeutic agent by inhibiting the initial step of glycolysis catalyzed by hexokinase, leading to the formation of 2-deoxyglucose-6-phosphate (2-DG-6P), which cannot be metabolized within cells (Supplementary Fig. 11a)[49]. In order to delineate the metabolic perturbation of cancer cells at the single-cell level, we compared the metabolic dynamics by isotope tracing of single MDA-MB-231 cells under normal or 2-DG drug treatment conditions, wherein separate pools of cells were set for each condition. Firstly, the 2-DG-6P was detected in single cells of drug treatment groups while the slight decrease of relative intensity in the overnight group may result from the leaking from the cell during cell aging (Supplementary Fig. 11b). Thus, the cell morphology was observed and the cell viability was determined to verify the cell integrity and viability after 2-DG treatment. (Supplementary Fig. 12). The concentration of assigned metabolites represented by the relative intensity was analyzed, and significantly different metabolites between 2-DG treatment with different treated times and control groups were hierarchical clustered (Supplementary Fig. 11c and Supplementary Data 3). Trend analysis revealed five main profiles of metabolite changes (Supplementary Fig. 11d), and the corresponding KEGG enrichment analysis was conducted (Supplementary Fig. 11e). The significant decrease of metabolites in profile 1 in the 2-DG treatment group, particularly the overnight treatment group, indicated the downregulation of amino sugar and nucleotide sugar metabolism, taurine and hypotaurine metabolism, ascorbate and aldarate metabolism, etc., following glycolysis inhibition. The metabolites in profiles 2-3 demonstrated the downregulation of purine metabolism, pentose phosphate pathway, and pyrimidine metabolism, indicating the downregulation of nucleotide biosynthesis resulting from both 2-DG treatment and cell aging. The metabolites in profile 4 exhibited a significant upregulation in both drug treatment groups, including arginine biosynthesis, starch and sucrose metabolism, fructose and mannose metabolism, etc., encompassing some amino acids as well as hexose and hexose phosphate, which probably accumulated due to the slowdown of the glucose consumption rate. In addition, it's worth noting that some metabolites in profile 1 and 5 showed elevated concentration in 3 h treatment group, such as phosphatidylethanolamines (PE) which was consistence with the existing study[50], sphingomyelin (SM) which closely associated with cell fates through SM/ceramide balance[51,52], and glutamine which probably served as an alternative carbon source to cope with the glycolysis inhibition during the initial stages of 2-DG treatment.

Concentration analysis provides a snapshot of metabolite abundance at a single time point, but this measurement cannot reflect the dynamic activity of metabolites. In contrast, dynamic single-cell metabolomics using isotope labeling offers valuable insights into metabolic activity. For instance, the 2-DG treatment can induce inhibition of glycolysis and downstream pathways, yet the abundance of UDP-glucose/UDP-galactose didn't show significant changes within the three groups (Fig. 6a, left panel). However, following the treatment containing 1 h labeling with [U-^{13}C]-glucose, the LE of UDP-glucose/UDP-galactose in three groups exhibited a declining trend (Fig. 6a, right panel), indicative of reduced glycolytic activity. Similarly, the abundance of UDP-GlcNAc remained unchanged after 3-hour treatment but significantly decreased following overnight treatment, suggesting the concentration downregulation only after prolonged exposure (Fig. 6b, left panel). However, the LE of UDP-GlcNAc displayed a marked decrease of LE in both of the treatment groups (Fig. 6b, right panel). The verification from bulk cells analyzed by LC-MS was demonstrated in Supplementary Fig 13a, b, strengthen the results from single cells. In addition, the LE of these metabolites after 2-DG treatment ranging from 1 h to 24 h indicated a rapid and sensitive time-dependent activity downregulation in glycolysis and associated pathways (Supplementary Fig. 14). Furthermore, the time-course labeling of these two metabolites within 3 h exhibited a decreased labeling rate under 2-DG treatment (Fig. 6c, d), in which isotope labeling commenced following either a 3 h or overnight 2-DG treatment. These results demonstrated the activity alteration reflected by LE of labeled metabolites under 2-DG treatment in single cells, especially after a short exposure, at which time the abundance may haven't change significantly.

Subsequently, the LE of labeled metabolites in three groups were hierarchically clustered, and two distinct clusters emerged (Fig. 6e). Labeled metabolites in cluster 1 exhibited decreased LE across the three groups, revealing that 2-DG inhibition not only reduced glycolysis activity, but also impacted associated pathways such as amino sugar and nucleotide sugar metabolism, galactose metabolism, etc., as well as purine metabolism which impacted by cell aging simultaneously as indicated by LE of bulk cells (Supplementary Fig. 13c). Conversely, the labeled metabolites in cluster 2 (Fig. 6e) exhibited increased metabolic activity in the alanine, aspartate and glutamate metabolism, TCA cycle, etc., following 2-DG treatment which might serve as alternative energy sources under glycolysis inhibition which verified by bulk cells either (Supplementary Fig. 3b and Supplementary Figs. 13c, d). Meanwhile, the concentration of all the above labeled metabolites in single cells exhibited a downregulation or no significant change. (Fig. 6f).

Furthermore, UMAP was performed on the labeled metabolites for dimensionality reduction of single cells under different conditions (Fig. 6g). When using relative intensity for dimensionality reduction, it proved challenging to distinguish between single cells in three groups. While with the information of LE of the labeled metabolites, the three groups were basically distinguished based on their different activity levels. In addition, better discrimination can be achieved using relative intensity of all metabolites with the addition of LE of labeled metabolites, especially between 2-DG treatment groups with different exposure duration (Fig. 6h). Consequently, dynamic single-cell metabolomics provided valuable activity information enabling fine and efficient single-cell clustering, serving as necessary complements for concentration analysis.

Cell-cell interactions between tumor cells and macrophages

TME is a sophisticated integrated network primarily comprised of tumor cells, immune cells, fibroblasts, and adjacent microvessels. Macrophages are pivotal constituents of TME and play crucial roles in tumor progression. They can reprogram their metabolomics induced by tumor cells and polarize into TAM, which in turn promote tumor progression and immune suppression[53]. Thus, investigating the intricate crosstalk between tumor cells and macrophages helps to understand the biological process within TME and find new strategies for cancer therapy.

Herein, the dynamic single-cell metabolomics system was employed to investigate the interactions between tumor cells and macrophages. Initially, mono-cultured MDA-MB-231 cells and macrophages derived from THP-1 cells were analyzed, revealing significantly different metabolites that were used for the UMAP cluster of single cells subsequently. The UMAP analysis demonstrated highly reproducible clustering of these two cell types with or without

https://doi.org/10.1038/s41467-025-59878-w

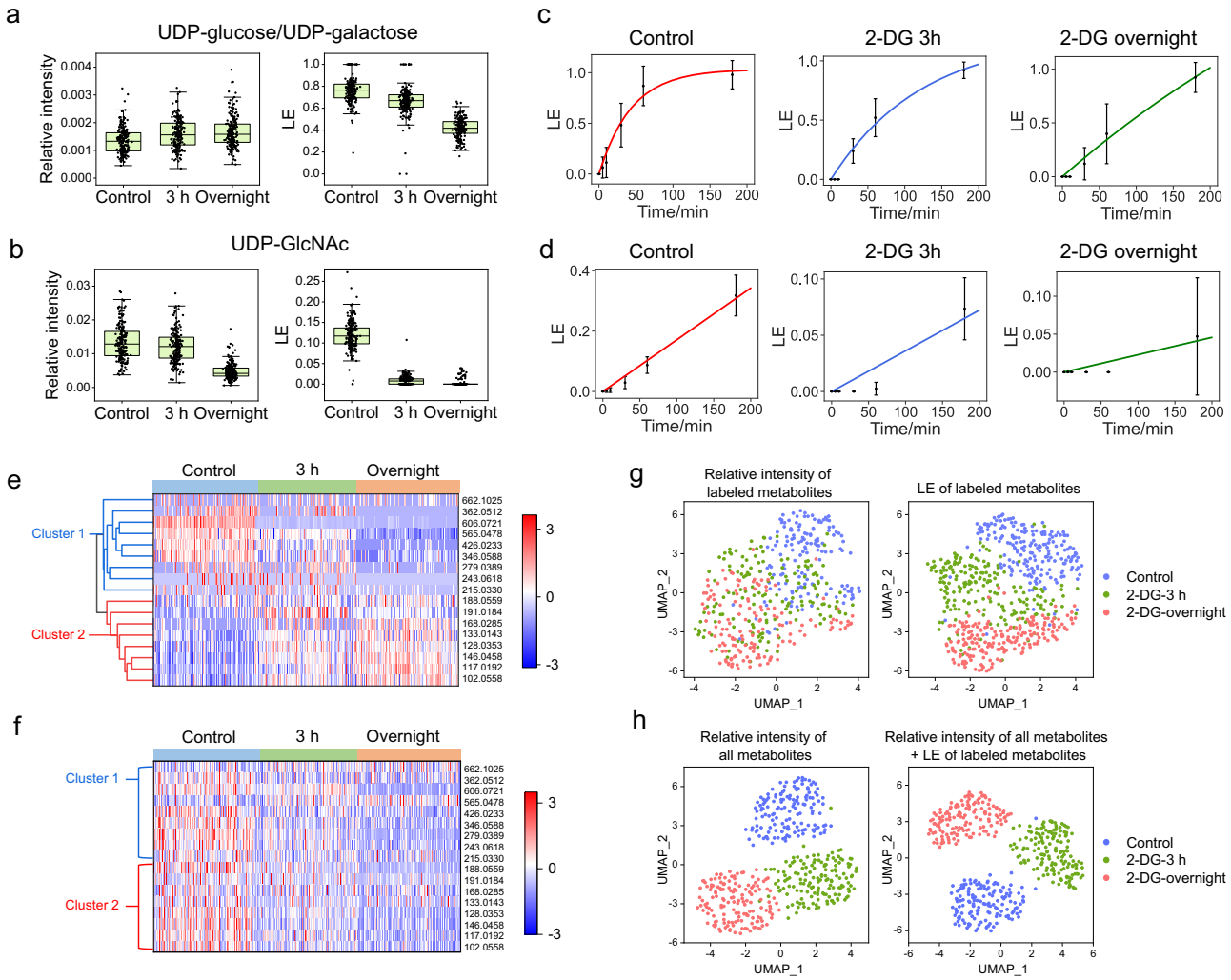

Fig. 6 | 2-DG induced metabolic activity perturbation and single-cell cluster analysis. a Relative intensity and LE of UDP-glucose/UDP-galactose in 3 groups. **b** Relative intensity and LE of UDP-GlcNAc in 3 groups. The centerlines of the boxplots indicate the median values, the lower and upper lines in boxplots correspond to 0.25 and 0.75 quartiles, and the whiskers indicate the largest and lowest points inside the range defined by 0.25 and 0.75 quartiles plus 1.5 times IQR. Cell number = 200 for each group. **c**, **d** The time-course labeling curve of (**c**) UDP-glucose/UDP-galactose and (**d**) UDP-GlcNAc in 3 groups. Data are presented as mean values (black dots) +/− SD. The lines represent the exponential fitting line. Cell number = 100 for each group. **e** Hierarchical clustering of Z-score normalized LE of labeled metabolites. **f** Heatmap of Z-score normalized relative intensity of labeled metabolites. Cell number = 200 for each group. **g** UMAP analysis of 3 groups based on relative intensity or LE of labeled metabolites. Cell numbers = 150 and 200 in the two panels, respectively. **h** The UMAP analysis of 3 groups based on the relative intensity of all metabolites with or without LE of labeled metabolites. Cell number = 150 for each group. Source data are provided as a Source Data file.

[U-^{13}C]-glucose labeling (Supplementary Fig. 15a), with the ability to precisely classify the mixture into different cell types (Supplementary Fig. 15b). Following co-culture for 3 days, single-cell metabolomic analysis revealed that the co-cultured cells could be classified into two clusters (purple dots in Fig. 7a), one of which closely overlapped with mono-cultured macrophages while the other partially overlapped with mono-cultured MDA-MB-231 with some deviation. Furthermore, co-cultured cells were labeled with CD45 antibody-APC fluorescent dyes and subjected to FACS for separation of tumor cells and macrophages, following by single-cell metabolomic analysis. The results demonstrated that CD45$^+$ cells overlapped with macrophages, whereas CD45$^-$ cells aligned with the deviated cluster of MDA-MB-231 in co-cultured samples (purple dots in Fig. 7a), confirming significant metabolic alterations in MDA-MB-231 cells after co-culture and demonstrating the feasibility of our single-cell metabolomics platform for direct analysis of co-cultured cells based on their metabolic features without requiring any labeling.

To facilitate more convenient and accurate classification of the two cell types in co-cultured samples for downstream analysis, a supervised machine learning model based on neural networks with three linear layers was developed (Fig. 7b and Supplementary Fig. 16a). The performance of the trained model was validated through 5-fold cross-validation, demonstrating its effectiveness (Fig. 7c and Supplementary Fig. 16b). The predicted results for the entire testing dataset and each subset of it are presented in Fig. 7d, e respectively, while the robustness and generalization capability were confirmed through biological repeats and macrophages treated by conditioned media of MDA-MB-231 cells (Supplementary Fig. 16c). Subsequently, the trained model was utilized for classifying co-cultured cells, with the predicted results shown in Fig. 7f.

Firstly, concentration analysis was performed on unlabeled samples, revealing significantly different metabolites between mono- and co-cultured cells (Supplementary Fig. 17a, b and Supplementary Data 4). In MDA-MB-231 cells, KEGG analysis indicated upregulation of glycerophospholipid metabolism, amino sugar and nucleotide sugar metabolism, fructose and mannose metabolism, pentose phosphate pathway, etc. Meanwhile, downregulation was observed in phenylalanine, tyrosine and tryptophan biosynthesis, alanine, aspartate and

https://doi.org/10.1038/s41467-025-59878-w

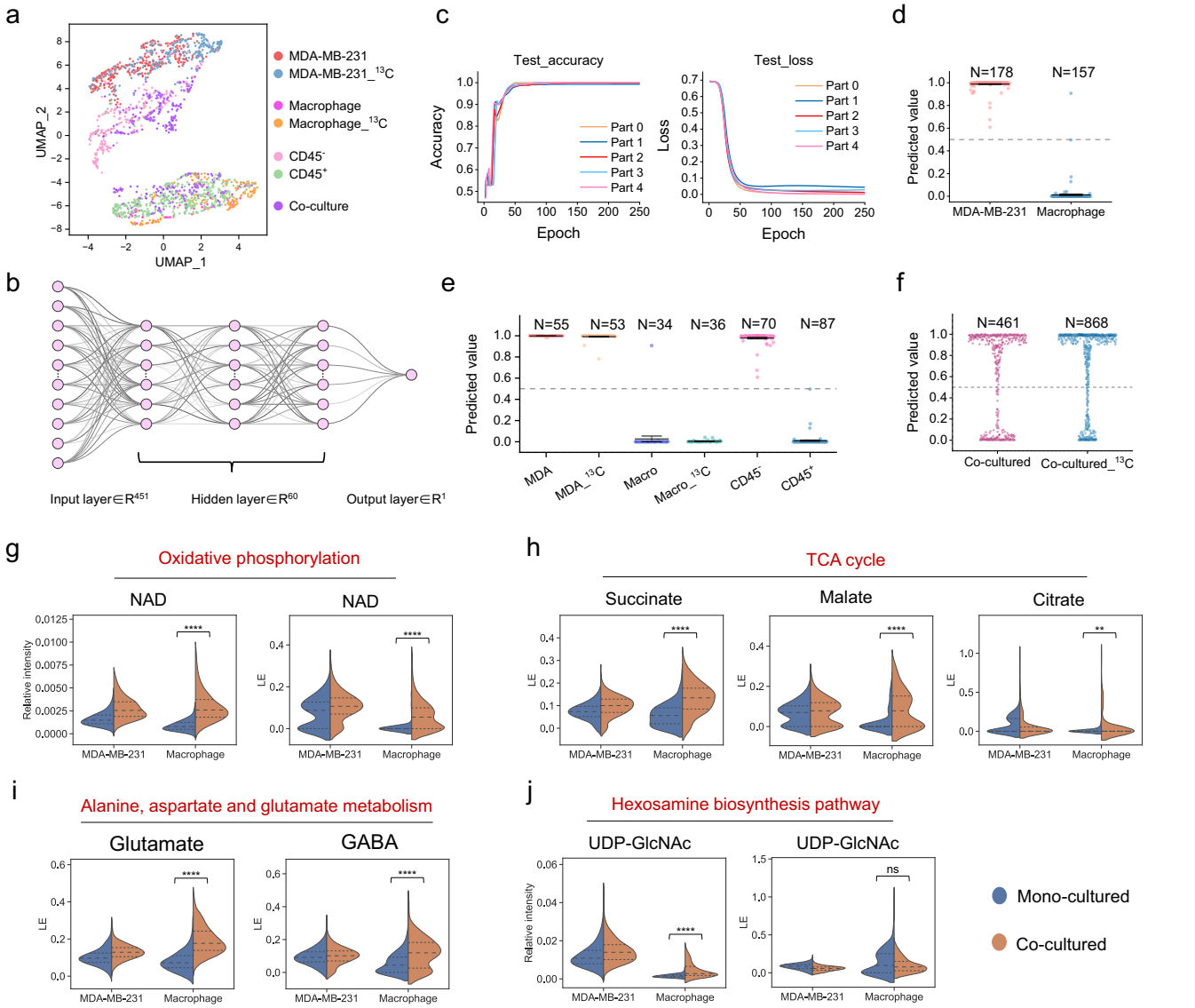

Fig. 7 | Metabolomic analysis of co-cultured MDA-MB-231 cells and macrophages. a The UMAP analysis of single cells. Cell number of MDA-MB-231 = 334, macrophage = 65, ^{13}C labeled MDA-MB-231 = 282, ^{13}C labeled macrophage = 204, $CD45^-$ = 297, $CD45^+$ = 470, co-culture = 327. The gating panels of FACS data are provided in Source Data. **b** The construction of the neural network model. **c** The accuracy and loss function of the testing dataset. **d**, **e** The predicted results of (**d**) the entire testing dataset and (**e**) subset of it. **f** The predicted results of co-cultured samples. **g**–**j** Concentration and activity alteration of co-cultured cells compared to mono-cultured ones. The median values, 0.25 and 0.75 quartiles are drawn as dotted lines on violin plots. A two-sided Wilcoxon rank-sum test was performed to access significance, and the *P*-value for groups with | Fold Change | > 2 were noted. $P = 2.94 \times 10^{-50}$ and 2.48×10^{-26} for the relative intensity changes of NAD and UDP-GlcNAc in macrophages, respectively. $P = 2.12 \times 10^{-32}$, 2.40×10^{-29}, 1.22×10^{-14}, 2.59×10^{-3}, 9.43×10^{-52}, 1.38×10^{-14} for the LE changes of NAD, succinate, malate, citrate, glutamate, and GABA in macrophages, respectively. $^*P < 0.05$, $^{**}P < 0.01$, $^{***}P < 0.001$, $^{****}P < 0.0001$; ns non-significant. Cell number of mono-cultured MDA-MB-231 = 794, ^{13}C labeled mono-cultured MDA-MB-231 = 833, mono-cultured macrophage = 245, ^{13}C labeled mono-cultured macrophage = 223, co-cultured MDA-MB-231 = 303, co-cultured macrophage = 158, ^{13}C labeled co-cultured MDA-MB-231 = 635, ^{13}C labeled co-cultured macrophage = 233. Source data are provided as a Source Data file.

glutamine metabolism and other amino acids pathways after co-culture (Supplementary Fig. 17c). The comparison of relative intensity of represent metabolites from these pathways between mono- and co-cultured MDA-MB-231 cells were displayed in Supplementary Fig. 18. For macrophages, upregulation was observed in pyrimidine metabolism, amino sugar and nucleotide sugar metabolism, taurine and hypotaurine metabolism, etc (Supplementary Fig. 17d). While some metabolites with downregulated abundance such as phosphoethanolamines were notated in Supplementary Fig. 17b. Likewise, the intensity alteration of corresponding metabolites was displayed in Supplementary Fig. 19.

Subsequently, the metabolic activity analysis was performed using 1 h [U-^{13}C]-glucose tracing, and significant activity alteration was observed in TAM. The upregulation of metabolic activities in TAM, including oxidative phosphorylation, amino sugar and nucleotide sugar metabolism, purine metabolism and arginine biosynthesis is consistent with the findings from concentration analysis (Fig. 7g and Supplementary Fig. 20). In addition, the metabolic activity in TCA cycle including succinate, malate and citrate was also up-regulated in TAM (Fig. 7h), as well as alanine, aspartate and glutamate metabolism, glutathione metabolism and serine biosynthesis (Fig. 7i and Supplementary Fig. 20), which without significant difference in their abundance. It worth to mention that the metabolic shift to oxidative phosphorylation and TCA cycle aligned with the reported metabolic alterations in M2 polarized macrophages, endowing TAM with predominant M2-like pro-tumor capabilities[53]. Interestingly, the

abundance of UDP-GlcNAc increased while its metabolic activity decreased marginally on the other side (Fig. 7j), suggesting the accumulation of UDP-GlcNAc in TAM at this stage may be attributed to its reduced consumption. UDP-GlcNAc promotes the O-GlcNAc glycosylation modifications of proteins, which reported to influence the inflammatory responses in macrophages and regulate the transformation between M1 and M2 polarization of TAM[54,55]. This warrants further investigation into its biological mechanisms. Overall, the integrated results from abundance and activity analysis reveal a metabolic reprogramming of direct co-cultured tumor cells and macrophages, including the increased hexose metabolism and pentose phosphate pathway while decreased glutamine metabolism and amino acids synthesis in MDA-MB-231 cells after direct interaction with macrophages, and the predominant M2-like polarization of TAM characterized by increased TCA cycle and oxidative phosphorylation, as well as other pathways which indicating a complex constitute of TAM in TME.

Macrophages have been classified into two main polarization states: M1 polarization, characterized by pro-inflammatory phenotype, and M2 polarization, characterized by anti-inflammatory phenotype. However, not all TAMs exhibit a clear M1 or M2 phenotype, as they often express markers associated with both polarization phenotypes[56,57], which underscores the need to delineate novel TAM phenotypes rather than the M1/M2 dichotomy. Recent studies have utilized single-cell RNA-sequencing (scRNA-Seq) technology to construct a new landscape of cell subpopulations according to the genomic characterization[58,59]. Here, a single-cell metabolomic platform provides a cell heterogeneous analysis of macrophages in TME characterized by diverse metabolic features. UAMP analysis according to metabolic activities was conducted for refined subtyping of TAM, and 4 subclusters emerged (Supplementary Fig. 21a). Cluster 1 and 2 demonstrated a higher activity in arginine biosynthesis (N-Acetyl-L-glutamic acid) and oxidative phosphorylation (NAD), while cluster 3 and 4 demonstrated a higher level of hexosamine biosynthesis pathway (UDP-GlcNAc), indicating a higher metabolic activity of mitochondrial metabolism in cluster 1 and 2 and a higher metabolic activity in hexose metabolism in cluster 3 and 4 (Supplementary Figs. 21b, c). In addition, cluster 1 and 2 were grouped by the different activity in lipopolysaccharide metabolism (Neu5Ac[60,61]), and cluster 3 and 4 were predominantly grouped by their difference in galactose metabolism (UDP-glucose) as shown in Supplementary Fig. 21d. Then, the metabolomics data was compared with scRNA-Seq data integrated from different tumor types[62] (Supplementary Fig. 22). Among the 12 clusters of macrophages based on gene features, the RTM_int subpopulation and the Mac_Angio subpopulation demonstrated enrichment in genes related to the oxidative phosphorylation pathway. Moreover, the RTM_int also displayed gene enrichment in glycolipid and glycan synthesis, which was consistent with the metabolic characteristics of clusters 1 and 2. This indicates their biological functions of inducing epithelial-mesenchymal transition and angiogenesis, respectively, according to the enrichment genes from scRNA-Seq data. In addition, the group of subpopulations encompassing Mac_IFN, RTM_IFN, and another group including Mac_Hypo, Mac_Alv-like, and RTM_LA all exhibited gene enrichment in glycolysis and nucleotide metabolism. Meanwhile, the latter group showed significantly higher enrichment in galactose metabolism, indicating the consistency of these two groups with clusters 3 and 4 in metabolomic analysis (Supplementary Fig. 22), suggesting the shared function of extracellular matrix remodeling of cluster 3/4 and the additional function of the interferon signaling pathway of cluster 4. In addition, subpopulations of macrophages corresponding to cluster 1/2/4 and Mac_Hypo in cluster 3 showed enrichment of genes associated with pro-tumor process, indicating the predominant pro-tumor function of TAM under direct co-culturing with tumor cells. Overall, the single-cell subtyping analysis revealed a heightened metabolic diversity among macrophages in TME, endowing them with various potential functions such as pro-tumor, angiogenesis, extracellular matrix remodeling, interferon signaling, etc[62].

Discussion

In this study, we developed a dynamic single-cell metabolomics system through the construction of a single-cell metabolomics data acquisition platform with the introduction of stable isotope tracing and the development of a dynamic single-cell data processing platform. Organic mass cytometry with high single-cell throughput was established for data acquisition, and a Python program was established for single-cell essential data processing and untargeted isotope tracing analysis, which equipped with unbiased peak quantification and robust characteristic peak extraction over background. 40 labeled metabolites under both negative and positive mode labeled by [U-^{13}C]-glucose and [U-^{13}C]-glutamine were traced in MDA-MB-231 single cells within 3 h, and the global metabolic activity profiling demonstrated various labeling rates of different pathways. The averaged isotope tracing data showed consistency with LC-MS analysis of bulk cells, while cell heterogeneous in metabolic activity was also unraveled using our method. The interconnection and flow of metabolic pathways was demonstrated by labeling patterns such as glycolysis pathway, pyrimidine metabolism, distinct TCA cycles, etc. In addition, correlation analysis between different pathways showed relationships consistency to the metabolic network. Furthermore, more pathways, such as gluconeogenesis and reductive metabolism, were observed by additional isotope tracers.

The metabolomics perturbation induced by 2-DG in breast cancer cells were further explored. Glycolysis downstream pathways, such as nucleotide sugar biosynthesis, showed significantly decrease in metabolic activity while remaining unchanged in abundance. The labeled metabolites with decreased concentrations in the TCA cycle, however, showed increased activities, which might serve as an alternative energy source under glycolysis inhibition. PCA revealed the differentiation of single cells between the control group and the 2-DG-treated groups based on their distinct LE, which cannot be distinguished by their relative intensity. These findings underscore the importance of conducting metabolic activity analysis as a valuable complement to concentration analysis. Significantly, to address the challenge in population cell analysis, single-cell metabolomic analysis was conducted for the direct cell-cell interaction analysis between tumor cells and macrophages. The direct co-culture of naïve macrophages (M0) and tumor cells in our experiment provided a model of the interaction between early infiltrated macrophages and tumor cells, which is less reported. There would be a conflict between the anti-tumor activity of M0 towards tumor cells and the TAM polarization of M0 impacted by tumor cell, which exhibits an opposite pro-tumor capability. After the effective cell typing with the aid of machine learning, the union analysis of concentration and activity demonstrated the enhancement of hexose metabolism and pentose phosphate pathway while decreased glutamine metabolism and amino acids synthesis in MDA-MB-231 cells after co-culture, as well as the predominant M2-like polarization of TAM characterized by increased oxidative phosphorylation and TCA cycle in TAM, disclosing a predominant transformation of M0 into a more M2-like TAM. And the metabolic alteration of MDA-MB-231 cells probably underwent suppression followed by promotion by macrophages under direct cell-cell contact between the two types of cells. In addition, there's other works revealed direct cell-cell contact may potentially influence M0 macrophages to support the TNBC cell line growth rather than inhibiting it, which contrasts with the outcomes observed when using conditioned medium[63]. These results highlight the significance of single-cell online metabolomic analysis, which enabling rapid online detection of direct co-culture of cells to better mimic physiological conditions in the TME in vivo. Furthermore, the refined subtyping of TAM revealed the heterogeneity of metabolic activities during polarization, indicating a

heightened metabolic diversity in TAM in the microenvironment besides the simplistic M1/M2 polarization.

In summary, a dynamic single-cell metabolomics system was proposed and successfully demonstrated by the global profiling of metabolic activity and flow analysis of metabolic pathways at the single-cell level. The significance of metabolic activity profiling for single-cell metabolomic analysis was underscored by a 2-DG inhibition model, which demonstrated sensitive metabolic activity alteration and fine intergroup clustering of single cells which cannot achieved by solely concentration analysis. The system showed great potential in the exploration of important biological issues at the single-cell level. Metabolic alteration of cell-cell interaction between tumor cells and macrophages was depicted from the union analysis of static and dynamic metabolomics, which further indicated more versatile polarization subtypes of TAM. As a result, dynamic single-cell metabolomics advances single-cell metabolomic analysis to a new dimension, offering great potential for enhanced comprehension of cell heterogeneity and contributing to future therapeutic implications.

Methods

Reagents and materials

MDA-MB-231 cells and A549 cells were obtained from Xinxiang Zhang Laboratory (Peking University), MCF10A cells were obtained from Chu Wang Laboratory (Peking University). MCF-7 cells were purchased from KeyGEN BioTECH (Jiangsu, China. Catalog # KGG3332-1). The human monocyte cell line THP-1 was acquired from ATCC (ATCC Number TIB-202). Dulbecco's Modified Eagle Medium (DMEM)/high glucose (+ 25 mM glucose, + 4 mM L-glutamine) were purchased from Thermo Fisher Scientific Life Technologies (USA). The dialyzed fetal bovine serum (dFBS) was purchased from Biological Industries (Kibbutz Beit-Haemek, Israel). The [U-^{13}C]-glucose, [U-^{13}C]-glutamine, [U-^{13}C]-lactate were purchased from Cambridge Isotopes Laboratories (MA, USA). CD45 monoclonal antibody (HI30), APC, eBioscience™ (Catalog # 17-0459-42) were purchased from Invitrogen.

Cell culture and pretreatment

The MDA-MB-231 cells and A549 cells were cultured in DMEM/high glucose medium supplemented with 10% dFBS, 80 μ/mL penicillin, and 80 μg/mL streptomycin. MCF-7 cells and THP-1 cells were cultured with RPMI-1640 medium supplemented with 10% dFBS, 80 U/mL penicillin, and 80 μg/mL streptomycin. MCF10A cells were culture in MEGM (Lonza, CC-3150) supplemented with 10% horse serum, 80 U/mL penicillin, and 80 μg/mL streptomycin. All of the cells were cultured in an incubator with 5% CO_2 at 37 °C.

For [U-^{13}C]-glucose labeling experiments, when cells were grown to 80% confluence, the unlabeled medium was removed, and cells were washed by PBS for 3 times. Then, glucose-free DMEM with 25 mM [U-^{13}C]-glucose and 10% dFBS was added for isotope labeling. For [U-^{13}C]-glutamine labeling, the medium was replaced by glutamine-free DMEM with 4 mM [U-^{13}C]-glutamine and 10% dFBS. For [U-^{13}C]-lactate labeling, the cells were cultured in DMEM/high glucose with 10 mM unlabeled lactate and 10% dFBS for 3 days, later the medium was replaced by DMEM/high glucose with 10 mM [U-^{13}C]-lactate and 10% dFBS for solely lactate labeling, replaced by glucose-free DMEM with 25 mM [U-^{13}C]-glucose, 10 mM unlabeled lactate and 10% dFBS for solely glucose labeling, or replaced by glucose-free DMEM with 25 mM [U-^{13}C]-glucose, 10 mM [U-^{13}C]-lactate and 10% dFBS for two tracers' labeling. After labeling, the labeling medium was quickly removed, and cells were washed twice by PBS, trypsinized, and dispersed in PBS. Cells were quickly placed in the dry ice until PBS was removed by centrifugation, and cells were resuspended in 140 mM ammonium formate aqueous solution (pH = 7.3). Then, cells were counted and diluted into 1×10^4/mL by ammonium formate buffer, followed by detection with organic mass cytometry immediately.

For co-culture experiments, THP-1 cells were treated with 100 ng/mL phorbol-12-myristate-13-acetate (PMA; Sigma–Aldrich, USA) for 48 h for differentiation into macrophages. Subsequently, macrophages were mixed with MDA-MB-231 cells at a ratio of 1:1 and co-cultured for 3 days. After co-culture, the co-cultured cells and mono-cultured cells were harvested by trypsin for FACS or direct single-cell metabolomic analysis. For the production of conditioned media from MDA-MB-231 cells, the MDA-MB-231 cells were washed by PBS when the cell confluence is around 80%, and were further cultured in fresh DMEM media for another 24 h. Then, the media were collected, filtered by 0.22-μm filters, and stored in 4 °C.

Construction of mass cytometry device

The construction was built refer to CyESI-MS, which was illustrated in Supplementary Fig. 1a, b. Briefly, the inner capillary (150 μm OD., 50 μm ID.) was used to introduce cell suspension, which was driven by a Pressure Injection Cell with Magnetic Stirplate (Next Advance, Inc. USA) with 15 psi. A curved segment of 5 loops with a total length of 23 cm was fabricated for cell ordering by Dean flow. Then, the inner capillary was wrapped by the middle capillary (360 μm OD., 200 μm ID.) through a metal three-way valve, which was utilized for sheath liquid transportation. High voltage was applied on the sheath liquid by a metal valve for electrospray ionization. The sheath gas was also introduced by a three-way valve and wrapped the middle capillary by a poly(ether-ether-ketone) capillary (790 μm OD., 500 μm ID.). At the tip of this device, the outlet of the inner capillary was 4 mm shorter than the middle capillary to achieve full contact of the cell suspension and sheath liquid for metabolites extraction and stable formation of electrospray. The outlet of the middle capillary was stretched out the outer capillary by 2 mm for nebulization, and nitrogen served as the sheath gas. For ddMS2 acquisition of single cells[36], the distance between the outlet of the inner capillary and the middle capillary was extended to 14 mm to prolong the contact time of the cell with methanol for the full release and diffusion of metabolites of single cells before their introduction into MS, thereby achieving an extended analysis window of single cells for ddMS2 acquisition.

Mass spectrometry for single-cell analysis

All mass spectrometry detection was performed on an Orbitrap MS (Q Exactive Plus, Thermo Scientific, San Jose, CA). The MS parameters for full MS acquisition were set as follows: capillary temperature = 320 °C, resolution = 35,000, AGC target = 1×10^6, maximum inject time = 50 ms, microscans = 1 in both positive and negative mode. The high voltage applied on sheath liquid was set as + 3.5 kV and − 3.5 kV in positive or negative mode, respectively. The MS parameters for ddMS2 mode acquisition were set as follows: resolution = 17,500, AGC target = 1×10^5, maximum inject time = 50 ms, isolation window = 0.4 Th, collision energy = 30,40,50, top N = 9, dynamic exclusion duration = 60 s.

Data analysis for single-cell essential data processing and isotope tracing

A streamline data processing platform was developed for single-cell essential data processing and isotope tracing. For essential data processing, 4 steps included:

(1) Single-cell pulse peak extraction: The raw MS data was transformed into mzML format by the MSConvert software (ProteoWizard). Then, the mzML file was read by a Python package named Pyteomics[64], and processed by a self-developed Python code. Briefly, the cell marker (m/z 306.0760) was used to extract single-cell events in the negative mode, and the intensity cutoff was set as 5×10^6. The continuous spectra with absolute intensity of m/z 306.0760 above the cutoff were assigned to one cell, and the spectrum of the maximum intensity of m/z 306.0760, the one spectrum before it, and the two spectra

after it were set as one cell pulse peak event. Thus, all cell pulses were extracted with each including a list of 4 spectra. In the positive ion mode, *m/z* 760.5844 was used as a cell marker, and the two spectra before its maximum spectrum, the one spectrum after it were set as one cell pulse peak event. In addition, the overlapped single-cell pulses were filtered out according to the interval between two cell pulses.

(2) Single-cell characteristic peak determination: firstly, the mass peaks with absolute intensity > 1e4 appeared in all single-cell pulses were extracted, and the peaks with occurrence frequency > 10% of all cells were filtered for further process. Secondly, all of these detected peaks went through maximum intensity extraction in each single-cell pulse, and the maximum intensity divided by the background intensity (defined as the former and the latter spectra, which were 2 spectra apart from the maximum) were record as the SBR. Only peaks with both SBR > 3 were defined as characteristic peaks in one cell. Finally, the characteristic peaks with occurrence frequency > 20% of all cells were filtered as characteristic peaks of single cells. For isotopologue searching, the threshold of occurrence frequency was setting for 15%.

(3) Metabolite annotation: the characteristic peaks detected in single cells were annotated to metabolites by accurate mass matching with standards in HMDB, local database, and MS/MS determined metabolites from population cells (MDA-MB-231) successively. For isotope tracing analysis, peaks with *m/z* < 663 were filtered for subsequent analysis.

(4) Intensity extraction from single cells: for isotope tracing analysis, the maximum intensities of all isotopologues of labeled metabolites (determined by isotope tracing analysis) were extracted. For normal analysis, the relative maximum intensities of all annotated metabolites were extracted.

For isotope tracing analysis, there were 5 steps after metabolite annotation described above, including isotopologue library construction, labeled peaks extraction, labeled metabolites determination, natural isotope correlation for isotopologues intensity and statistical analysis.

(1) Isotopologue library construction: after the metabolite annotation, the theoretical *m/z* of all isotopologues were calculated according to the carbon number of metabolites.

(2) Labeled peaks extraction: all characteristic peaks in the labeled or unlabeled single-cell samples were screened through the isotopologues library, and the detected isotopologue peaks were conserved.

(3) Labeled metabolites determination: the detected isotopologue peaks of labeled and unlabeled samples were compared, and the peaks which appeared in labeled samples and deficient in unlabeled samples were marked as labeled isotopologues. Finally, the corresponding labeled metabolites and labeled forms were determined.

(4) Intensity extraction and natural isotope abundance correlation: The absolute intensity of all isotopologues of labeled metabolites in each single cell were extracted, and natural isotope abundance correction was performed using the R package "AccuCor" (version 0.2.4; https://github.com/XiaoyangSu/AccuCor).

(5) After the labeled metabolites determination and peak intensity extraction, the data was proceeded for statistical analysis. The LE of each labeled form of metabolites was calculated, and the box plots of single-cell distribution were outputted. The averaged LE and the standard deviation of each labeled form of metabolites between single cells were calculated, and the averaged LE at all time points were fitted to the following exponential function[38], where *k* is the first-order rate constant, indicating the labeling rate of the metabolites from the tracer. Therefore, the time-course plots and corresponding fitting lines were outputted for each labeled form of metabolites. In addition, the labeling pattern of each metabolite in single cells were also outputted and analyzed.

$$LE = a \times e^{(-kt)} - a(a<0) \quad (1)$$

LC-MS analysis

(1) Sample preparation. For the isotope labeling experiment, when cells grown to 80% confluency, they were washed by PBS for 3 times, and DMEM containing 25 mM [U-^{13}C]-glucose was added and labeling for 1 or 3 h. After labeling, cells were harvested by either trypsinization or scraping. For trypsinization, cells were washed by PBS for 3 times, and 2 mL trypsin was added and incubated for 1 min for MDA-MB-231 cells. Then, the trypsinization was quenched by dFBS immediately, and the cells were blown down and collected by centrifugation. The cell pellet was washed by 5 mL PBS for 3 times, and 3 mL -20 °C pre-cooled 50% MeOH/H_2O was added for quenching and extraction of metabolites. For scraping, cells were washed by PBS for 3 times, and 3 mL -20 °C pre-cooled 50% MeOH/H_2O was added immediately, and cells were scraped from the plate and collected. After cell harvest, the samples were vortexed for 1 min followed by sonication for 10 min in an ice-bathed ultrasonic cleaner (40 kHz), and were centrifuged for 20 min using 16,200 g at 4 °C. The supernatant was evaporated to dryness in a vacuum concentrator. Dry extracts were saved at − 80 °C or reconstituted in 100 µL of ACN:MeOH:H_2O (3:2:1, v/v/v), followed by 10 min ice-bathed sonication (40 kHz) and 20 min centrifugation using 16,200 g at 4 °C. Supernatants were finally transferred to HPLC glass vials for LC-MS analysis. Biological replicates = 3 for the above trypsinization/scraping experiments. QC samples were prepared through the combination of unlabeled samples.

(2) LC separation. Metabolomics data was acquired using a UPLC system (Waters ACQUITY UPLC, Waters) coupled to an orbitrap MS (Q Exactive plus, Thermo Scientific). Waters ACQUITY UPLC BEH Amide column (particle size, 1.7 µm; 100 mm (length) × 2.1 mm (i.d.)) was used for LC separation for polar extraction of cell metabolites. Mobile phases A = 95:5 H_2O/ACN (v/v) containing 1‰ formic acid for positive mode / 95:5 H_2O/ACN (v/v) containing 1‰ $NH_3{\cdot}H_2O$ for negative mode. Mobile phases B = 100% ACN containing 1‰ formic acid for positive mode / 100% ACN containing 1‰ $NH_3{\cdot}H_2O$ for negative mode. Flow rate = 0.5 mL/min. The linear gradient eluted from 3% A (0-1 min), to 10% A (1–6 min), to 50% A (6–20 min), stayed at 50% (20-25 min) and went back to 3% A (25–30 min) for both positive and negative mode.

(3) Mass spectrometry. The MS parameters for full MS acquisition were set as follows: capillary temperature = 350 °C, resolution = 70,000, AGC target = 1×10^6, maximum inject time = 200 ms, aux gas heater temperature = 350 °C, sheath gas = 35 arb, aux gas = 10 arb; sweep gas = 5, scan range = 80–1200 Th, spray voltage = 3.5 kV or − 4.0 kV, in positive or negative modes, respectively. The MS parameters for ddMS2 acquisition were set as follows: resolution = 35,000, AGC target = 1×10^5, maximum inject time = 200 ms, isolation window = 0.4 Th, collision energy = 20,30,40, top *N* = 9, dynamic exclusion duration = 30 s.

(4) Data processing. The ddMS2 raw data acquired from Orbitrap MS was analyzed by Compound Discoverer 3.3 for metabolite annotation to construct a local library with MS/MS data for the MDA-MB-231 cell line. For bulk isotope tracing analysis, the full

scan raw data was transformed into mzXML format using MSConvert (ProteoWizard). Then, the mzXML files were processed by XCMS for peak detection, retention time correction, and peak grouping. The key parameters were set as follows: method = "centWave", ppm = 15, snthr = 10, peakwidth = c(5,60); minfrac, 0.5. Target extraction of labeled isotopologues was achieved by self-developed Python code, and natural abundance correction was performed using the R package "AccuCor" (version 0.2.4).

Calculation of labeling extent (LE)

Labeling extent (LE) represents the labeling enrichment of all labeling forms of one metabolite, or the labeling enrichment of one typical labeling form (Mn) if specifically annotated. It's calculated by Eq. (2).

$$LE = \frac{\sum_{i=1}^{n} I_{Mi}}{\sum_{i=0}^{n} I_{Mi}} \quad (2)$$

Fluorescence-activated Cell Sorting

FACS was performed on an Aria SORP flow cytometer (BD Biosciences). The samples were prepared according to the Flow Cytometry Protocols provided on the official ThermoFisher Scientific website. Briefly, the cells were harvested by trypsin and resuspended into 3% BSA/PBS solution. 5 μL antibody were added into 50 μL cell suspension and diluted into a final volume of 100 μL. The mixtures were incubated on ice in the dark for 30 min. Subsequently, the stained cells were washed, resuspended in 3% BSA/PBS solution, and analyzed as soon as possible.

Statistical analysis

The UMAP analysis was performed on the OmicShare online platform, and the parameters were set as follows: n_neighbors = 15, n_components = 2, metric = "Euclidean", n_epochs = 200, min_dist = 0.1 or 0.5, and negative_sample_rate = 5. The hierarchical clustering was performed on Origin and the parameters were set as follows: cluster method = "Group Average", distance type = "Euclidean".

Reporting summary

Further information on research design is available in the Nature Portfolio Reporting Summary linked to this article.

Data availability

The metabolomic MS raw data have been deposited to MetaboLights with the dataset identifier MTBLS11091. The published datasets related to the conclusions in this paper can be accessed under GEO accession numbers: GSE114727, GSE139829, GSE154600, GSE115978, GSE118390, GSE125449, GSE15803, GSE130973, GSE115978, GSE127465; URLs for additional data are https://www.synapse.org/#!Synapse:syn21560407 and http://blueprint.lambrechtslab.org, as well as https://support.10xgenomics.com/single-cell-gene-expression/datasets/1.1.0/pbmc3k. The integrated datasets can be downloaded through the following link: https://cellxgene.cziscience.com/collections/3f7c572c-cd73-4b51-a313-207c7f20f188 provided by https://doi.org/10.1038/s41467-024-49916-4. All data supporting the present study are available within the paper and the Supplementary Information. Source data are provided in this paper.

Code availability

The code developed in this manuscript has been submitted to Code Ocean, https://doi.org/10.24433/CO.6142726.v1.

References

1. Sinclair, E. et al. Metabolomics of sebum reveals lipid dysregulation in Parkinson's disease. *Nat. Commun.* **12**, 1592 (2021).
2. Auger, J. P. et al. Metabolic rewiring promotes anti-inflammatory effects of glucocorticoids. *Nature* **629**, 184–192 (2024).
3. Zamboni, N., Saghatelian, A. & Patti, G. J. Defining the metabolome: Size, flux, and regulation. *Mol. Cell* **58**, 699–706 (2015).
4. Fernández-García, J., Altea-Manzano, P., Pranzini, E. & Fendt, S. M. Stable isotopes for tracing mammalian-cell metabolism. *Trends Biochem. Sci.* **45**, 185–201 (2020).
5. Xu, Y. F. et al. Regulation of yeast pyruvate kinase by ultrasensitive allostery independent of phosphorylation. *Mol. Cell* **48**, 52–62 (2012).
6. Yu, D., Zhou, L. A., Liu, X. Y. & Xu, G. W. Stable isotope-resolved metabolomics based on mass spectrometry: Methods and their applications. *TrAC, Trends Anal. Chem.* **160**, 116985 (2023).
7. Jang, C., Chen, L. & Rabinowitz, J. D. Metabolomics and isotope tracing. *Cell* **173**, 822–837 (2018).
8. Liang, L. F., Sun, F., Wang, H. B. & Hu, Z. P. Metabolomics, metabolic flux analysis and cancer pharmacology. *Pharmacol. Ther.* **224**, 107827 (2021).
9. Park, G. et al. Quantitative analysis of metabolic fluxes in brown fat and skeletal muscle during thermogenesis. *Nat. Metab.* **5**, 1204–1220 (2023).
10. Stern, A. et al. Inferring mitochondrial and cytosolic metabolism by coupling isotope tracing and deconvolution. *Nat. Commun.* **14**, 7525 (2023).
11. Huang, X. J. et al. XCMS: Global tracking of isotopic labels in untargeted metabolomics. *Anal. Chem.* **86**, 1632–1639 (2014).
12. Capellades, J. et al. geoRge: A computational tool to detect the presence of stable isotope labeling in LC/MS-based untargeted metabolomics. *Anal. Chem.* **88**, 621–628 (2016).
13. Hoffmann, F., Jaeger, C., Bhattacharya, A., Schmitt, C. A. & Lisec, J. Nontargeted identification of tracer incorporation in high-resolution mass spectrometry. *Anal. Chem.* **90**, 7253–7260 (2018).
14. Bahar, R. et al. Increased cell-to-cell variation in gene expression in ageing mouse heart. *Nature* **441**, 1011–1014 (2006).
15. Budnik, B., Levy, E., Harmange, G. & Slavov, N. SCoPE-MS: mass spectrometry of single mammalian cells quantifies proteome heterogeneity during cell differentiation. *Genome Biol.* **19**, 161 (2018).
16. Lun, X. K. et al. Influence of node abundance on signaling network state and dynamics analyzed by mass cytometry. *Nat. Biotechnol.* **35**, 164–172 (2017).
17. Colegio, O. R. et al. Functional polarization of tumour-associated macrophages by tumour-derived lactic acid. *Nature* **513**, 559–563 (2014).
18. Wang, Y. Z. et al. M2 Tumor-associated macrophages-derived exosomal promotes glycolysis and gastric cancer progression. *Adv. Sci.* **11**, 2309298 (2024).
19. Roehlecke, C. & Schmidt, M. H. H. Tunneling nanotubes and tumor microtubes in cancer. *Cancers* **12**, 857 (2020).
20. Zhong, Z. Y. et al. Tumor-associated macrophages drive glycolysis through the IL-8/STAT3/ GLUT3 signaling pathway in pancreatic cancer progression. *Cancer Lett.* **588**, 216784 (2024).
21. Binek, A. et al. Flow cytometry has a significant impact on the cellular metabolome. *J. Proteome Res.* **18**, 169–181 (2019).
22. Llufrio, E. M., Wang, L. J., Naser, F. J. & Patti, G. J. Sorting cells alters their redox state and cellular metabolome. *Redox Biol.* **16**, 381–387 (2018).
23. Chen, X. X., Peng, Z. K. & Yang, Z. B. Metabolomics studies of cell-cell interactions using single cell mass spectrometry combined with fluorescence microscopy. *Chem. Sci.* **13**, 6687–6695 (2022).
24. Feng, S., Zhang, Q., Xie, T. Z., Hou, Y. & Lin, J. M. In-situ monitoring calcium signaling through tumor microtubes for single cell-cell communication via an open microfluidic probe. *Biosens. Bioelectron.* **206**, 114137 (2022).
25. Wang, L. et al. Spatially resolved isotope tracing reveals tissue metabolic activity. *Nat. Methods* **19**, 223–230 (2022).

26. Wang, G. Q. et al. Analyzing cell-type-specific dynamics of metabolism in kidney repair. *Nat. Metab.* **4**, 1109–1118 (2022).
27. Miller, A. et al. Spatially resolved metabolomics and isotope tracing reveal dynamic metabolic responses of dentate granule neurons with acute stimulation. *Nat. Metab.* **5**, 1820–1835 (2023).
28. Schwaiger-Haber, M. et al. Using mass spectrometry imaging to map fluxes quantitatively in the tumor ecosystem. *Nat. Commun.* **14**, 2876 (2023).
29. Xu, S. T., Liu, M. X., Bai, Y. & Liu, H. W. Multi-dimensional organic mass cytometry: Simultaneous analysis of proteins and metabolites on single cells. *Angew. Chem. Int. Ed.* **60**, 1806–1812 (2021).
30. Xu, S. T., Xue, J. J., Bai, Y. & Liu, H. W. High-throughput single-cell immunoassay in the cellular native environment using online desalting dual-spray mass spectrometry. *Anal. Chem.* **92**, 15854–15861 (2020).
31. Yao, H. et al. Label-free mass cytometry for unveiling cellular metabolic heterogeneity. *Anal. Chem.* **91**, 9777–9783 (2019).
32. Shen, Z. Z. et al. Dynamic metabolic change of cancer cells induced by natural killer cells at the single-cell level studied by label-free mass cytometry. *Chem. Sci.* **13**, 1641–1647 (2022).
33. Xu, S. T., Yang, C. & Yan, X. P. Organic mass cytometry discriminating cycle stages of single cells with small molecular indicators. *Anal. Chem.* **95**, 2312–2320 (2023).
34. Pan, S. Y. et al. Single-cell metabolite profiling enables information-rich classification of lymphocyte types and subtypes. *Chem. Commun.* **60**, 392–395 (2024).
35. Qin, S. J., Miao, D. Y., Zhang, X., Zhang, Y. & Bai, Y. Methods developments of mass spectrometry based single cell metabolomics. *TrAC, Trends Anal. Chem.* **164**, 117086 (2023).
36. Qin, S. J. et al. In-depth organic mass cytometry reveals differential contents of 3-hydroxybutanoic acid at the single-cell level. *Nat. Commun.* **15**, 4387 (2024).
37. Huang, Q. S., Mao, S. F., Khan, M., Zhou, L. & Lin, J. M. Dean flow assisted cell ordering system for lipid profiling in single-cells using mass spectrometry. *Chem. Commun.* **54**, 2595–2598 (2018).
38. Wang, R. H. et al. Global stable-isotope tracing metabolomics reveals system-wide metabolic alternations in aging. *Nat. Commun.* **13**, 3518 (2022).
39. Wei, Z. W. et al. Rapid removal of matrices from small-volume samples by step-voltage nanoelectrospray. *Angew. Chem. Int. Ed.* **52**, 11025–11028 (2013).
40. Li, G. Y., Yuan, S. M., Pan, Y., Liu, Y. Z. & Huang, G. M. Binding states of protein-metal complexes in cells. *Anal. Chem.* **88**, 10860–10866 (2016).
41. Warburg, O. On the origin of cancer cells. *Science* **123**, 309–314 (1956).
42. DeBerardinis, R. J., Lum, J. J., Hatzivassiliou, G. & Thompson, C. B. The biology of cancer: metabolic reprogramming fuels cell growth and proliferation. *Cell Metab.* **7**, 11–20 (2008).
43. Gkiouli, M., Biechl, P., Eisenreich, W. & Otto, A. M. Diverse roads taken by ^{13}C-glucose-derived metabolites in breast cancer cells exposed to limiting glucose and glutamine conditions. *Cells* **8**, 1113 (2019).
44. Buescher, J. M. et al. A roadmap for interpreting ^{13}C metabolite labeling patterns from cells. *Curr. Opin. Biotechnol.* **34**, 189–201 (2015).
45. Leithner, K. et al. PCK2 activation mediates an adaptive response to glucose depletion in lung cancer. *Oncogene* **34**, 1044–1050 (2015).
46. Kalemba, K. M. et al. Glycerol induces G6pc in primary mouse hepatocytes and is the preferred substrate for gluconeogenesis both in vitro and in vivo. *J. Biol. Chem.* **294**, 18017–18028 (2019).
47. Metallo, C. M. et al. Reductive glutamine metabolism by IDH1 mediates lipogenesis under hypoxia. *Nature* **481**, 380–384 (2012).
48. Mullen, A. R. et al. Reductive carboxylation supports growth in tumour cells with defective mitochondria. *Nature* **481**, 385–388 (2012).
49. Dai, S. N. et al. Glycolysis promotes the progression of pancreatic cancer and reduces cancer cell sensitivity to gemcitabine. *Biomed. Pharmacother.* **121**, 109521 (2020).
50. Le Pogam, P. et al. Untargeted metabolomics reveal lipid alterations upon 2-deoxyglucose treatment in human HaCaT keratinocytes. *J. Proteome Res.* **17**, 1146–1157 (2018).
51. Hannun, Y. A. & Obeid, L. M. Sphingolipids and their metabolism in physiology and disease. *Nat. Rev. Mol. Cell Bio.* **19**, 175–191 (2018).
52. Taniguchi, M. & Okazaki, T. Role of ceramide/sphingomyelin (SM) balance regulated through "SM cycle" in cancer. *Cell. Signal.* **87**, 110119 (2021).
53. Liu, J. & Cao, X. T. Glucose metabolism of TAMs in tumor chemoresistance and metastasis. *Trends Cell Biol.* **33**, 967–978 (2023).
54. Jiang, G. Y. et al. Glycolysis regulation in tumor-associated macrophages: Its role in tumor development and cancer treatment. *Int. J. Cancer* **154**, 412–424 (2024).
55. Chang, Y. H., Weng, C. L. & Lin, K. I. O-GlcNAcylation and its role in the immune system. *J. Biomed. Sci.* **27**, 57 (2020).
56. Mantovani, A., Biswas, S. K., Galdiero, M. R., Sica, A. & Locati, M. Macrophage plasticity and polarization in tissue repair and remodelling. *J. Pathol.* **229**, 176–185 (2013).
57. Sanchez, L. R. et al. The emerging roles of macrophages in cancer metastasis and response to chemotherapy. *J. Leukoc. Biol.* **106**, 259–274 (2019).
58. Li, S. S. et al. Metabolism drives macrophage heterogeneity in the tumor microenvironment. *Cell Rep.* **39**, https://doi.org/10.1016/j.celrep.2022.110609 (2022).
59. Ochocka, N. et al. Single-cell RNA and protein sequencing reveals functional heterogeneity of glioma-associated brain macrophages. *Glia* **69**, E551–E552 (2021).
60. Huang, H. W. et al. CMAHP promotes metastasis by reducing ubiquitination of Snail and inducing angiogenesis via GM-CSF overexpression in gastric cancer. *Oncogene* **41**, 159–172 (2022).
61. Mortezai, N. et al. Tumor-associated Neu5Ac-Tn and Neu5Gc-Tn antigens bind to C-type lectin CLEC10A (CD301, MGL). *Glycobiology* **23**, 844–852 (2013).
62. Guimaraes, G. R. et al. Single-cell resolution characterization of myeloid-derived cell states with implication in cancer outcome. *Nat. Commun.* **15**, 5694 (2024).
63. Jumat, N. R. et al. The proliferation of MDA-MB-231 cells is repressed by mesenchymal stem cell-mediated macrophage activation conditioned medium through the inhibition of AKT1 and YKL-39 genes. *Biomed. Res. Ther.* **11**, 6737–6753 (2024).
64. Goloborodko, A. A., Levitsky, L. I., Ivanov, M. V. & Gorshkov, M. V. Pyteomics-a Python framework for exploratory data analysis and rapid software prototyping in proteomics. *J. Am. Soc. Mass Spectrom.* **24**, 301–304 (2013).

Acknowledgements

This work was financially supported by the Natural Science Foundation of China (No. 22125401 to Y.B.) and the National Key R&D Program of China (2022YFC3400700 and 2023YFF1205900 to Y.B.).

Author contributions

Y.B. proposed the study concept and strategy. Y.Z. and Y.B. designed and performed the experiments and data analysis. M.Y.S. contributed to the single-cell data acquisition experiments and the LC-MS data acquisition experiments. M.X.L. contributed to the LC-MS data acquisition experiments. S.J.Q. helped with the single-cell data acquisition experiments. D.Y.M. provided with LC-MS data acquisition method. M.Y.S., M.X.L., S.J.Q., and D.Y.M. provided with helpful discussion. Y.Z. and Y.B. wrote the paper.

Competing interests
The authors declare no competing interests.

Additional information
Supplementary information The online version contains supplementary material available at https://doi.org/10.1038/s41467-025-59878-w.

Correspondence and requests for materials should be addressed to Yu Bai.

Peer review information *Nature Communications* thanks Kyle Duncan, Lei Jiang, and the other anonymous reviewer(s) for their contribution to the peer review of this work. A peer review file is available.